POAC'13
Espoo, Finland

Proceedings of the 22nd International Conference on
Port and Ocean Engineering under Arctic Conditions
June 9-13, 2013
Espoo, Finland

Using distributed optical fiber sensors based on FBGs for the measurement of temperature fluctuations in saline ice and water on small scales

Aleksey Marchenko[1,2], David Wrangborg[2,1], Torsten Thiel[3]

[1] The University Centre in Svalbard, Longyearbyen, Norway

[2] Sustainable Arctic Marine and Coastal Technology (SAMCoT), Centre for Research-based Innovation (CRI), Norwegian University of Science and Technology, Trondheim, Norway

[3]Advanced Optics Solutions (AOS) GmbH, Dresden, Germany

Abstract
Registration of ice and water temperature around the interface is important for the understanding of the physical processes accompanying ice growth and melt processes such as convection, super cooling, migration of liquid brine through the ice etc. Temperature sensors for that approach generally should be much smaller than the ice thickness, in order to avoid negative feedback effects on the processes by the sensor's thermal capacity and/or conductivity. In our experiments, we used a novel fiber-optical thermistor string of an unprecedented thickness of 1 mm, containing 12 equidistant Fiber Bragg Grating sensors. The experiments were organized in the cold laboratory of UNIS for the modeling of thermal changes in confined ice below the coal quay Kapp Amsterdam in Svalbard. Temperature changes inside ice caused by the variations of the under ice water pressure were detected both in the field and laboratory experiments. FBG strain and temperature sensors were used to study thermal expansion of saline and fresh ice in the laboratory conditions. The experiments were performed with different rates of the air temperature variations in the cold laboratory.

Introduction

Typical element of coastal structures is a cofferdam. Cofferdams are used for the fastening of structural elements of quays and dams. It is known that coastal erosion can influence significant movements of unprotected shorelines in the Arctic. Cofferdam is standard protection for the pipelines crossing a shoreline (Fig 1a). Cofferdams are also used for the fastening of structural elements of stationary quays (Fig. 2a). The use of cofferdams in the Arctic conditions is associated with deformations of sheet pilings making constructions unstable after certain exploitation time. Understanding of physical processes and loads on cofferdams in coastal zones is important for the elaboration of new technical methods increasing sustainability of the coastal infrastructure in the Arctic.

The analysis of ice actions and deformations of the coal quay Kapp Amsterdam in Svalbard was performed in the papers (Løset and Marchenko, 2009; Marchenko et al., 2011; Sinitsin et al., 2012). It was concluded that deformations of the sheet piling of the quay can be explained by the thermal expansion of sea ice frozen to the sheet piling. Nevertheless the thermal expansion itself can't explain big displacements of the sheet piling in horizontal directions, and gradual migration of sea water through the ice inside the cofferdam should be accounted for the explanation of big deformations. Migration of sea water through the ice in vertical direction influences temperature variations over the ice column when vertical temperature

gradient is significant. For example the ice temperature should increase when warmer water from below the ice moves up in the porous space. Therefore temperature measurements inside the ice and water pressure measurements below the ice could give useful information about conditions and intensity of the water migration through the ice.

The ice tank in the cold laboratory of UNIS was used for the laboratory experiments. The ice frozen to the tank walls imitates the ice frozen to a cofferdam. Preliminary laboratory experiments performed in the cold laboratory of UNIS (Marchenko et al., 2011) demonstrated an increase of ice surface temperature due to the increase of the water pressure below the ice. Temperature measurements were performed with IR camera IR Flex, and the water pressure was risen up by the air pumping in submerged balloon. In the present paper we perform results of similar laboratory experiments where the ice temperature is detected with a novel fiber-optical thermistor string of an unprecedented thickness of 1 mm, containing 12 equidistant Fiber Bragg Grating (FBG) sensors. Results of previous field experiments are also analyzed to demonstrate similar effects observed in the full scale. The results on laboratory measurements of the coefficient of thermal expansion of saline and fresh water ice are also presented. Results of first experiments on thermal expansion of saline and fresh ice using FBG sensors were published by Marchenko et al. in 2012. In the latest experiments the deformation and temperature of ice samples were registered with the same FBG strain sensors and novel FBG thermistor string. It gave possibility to control temperature gradient inside the ice during the experiment.

a) b)

Figure 1. Construction of the cofferdam for the gas pipeline crossing in the Baydara Bay (from http://globalmd.ru/projects) (a), reconstruction of the quay in Svalbard in 2000 (from www.afgruppen.com).

Thermal changes inside floating saline ice induced by the water pressure variations

The scheme of the laboratory experiment is shown in Fig. 2a. The sizes of the ice tank are 1.2m x 1m x 0.5m. The ice in the tank was formed due to the cooling of the water surface The water consisted of the mixture of 60 cm sea water layer with 50 cm of fresh water layer. The sea water salinity was about 30 ppt. The mean salinity of the mixture is 13.6 ppt, and the mean freezing point of the mixture is -0.73^{o}C. Temperature over the top layer of the water and ice with thickness 12-11 cm was registered by the FBG thermistor string with 12 equidistant temperature sensors located on 1 cm distance from each other. The description of the work principles of FBG sensors are given in the Appendix. The resolution of temperature measurements is 0.08^{o}C. The thermistor string was fixed vertically in the ice tank when the

ice thickness was less than 1 cm (Fig. 3a). Sensor 1 was slightly above the ice surface and sensor 12 was almost on 12 cm depth in the water (Fig. 2a).

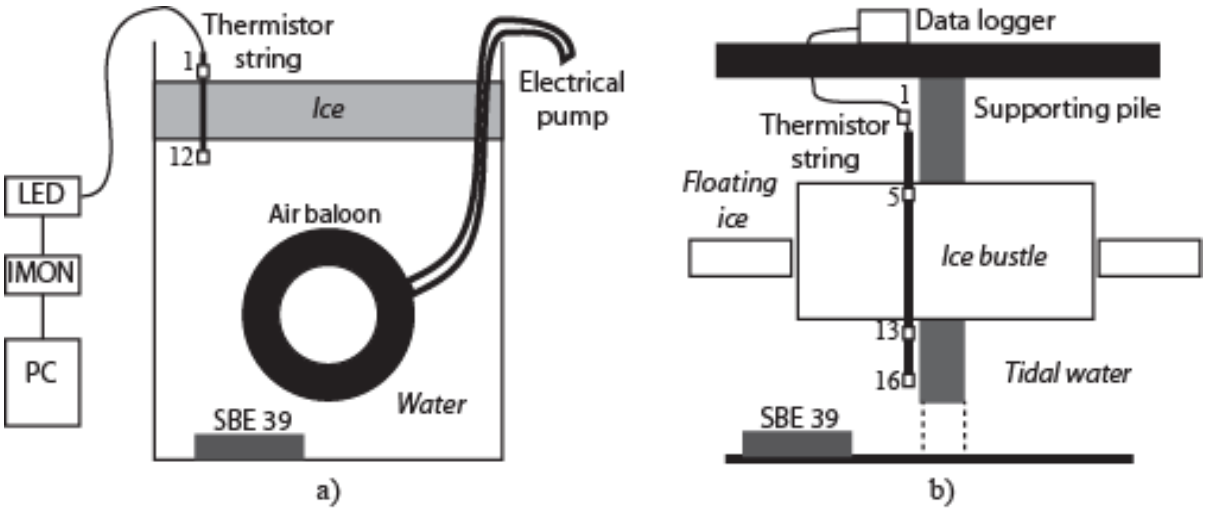

Figure 2. Schemes of laboratory experiment in the ice tank (a) and field experiment in the coal quay Kapp Amsterdam (b).

Temperature profiles recorded by the thermistors during 24 hours after the beginning of the ice growth are shown in Fig. 4. Dashed lines show vertical location of points with the temperature -0.6^{o}C. The ice thickness during this time was not measured. Assuming that the temperature of the ice bottom is at the freezing point we conclude that the ice thickness is between 1 and 2 cm in Fig. 4a, between 2 and 3 cm in Fig. 4b, around 4 cm in Fig. 4c, and below 7 cm in Fig. 4d. There was a layer of warm water on the top, and sensor 9 is at the low boundary of the warm water layer. The warm layer is almost absent in Fig. 4d. Below the ice bottom temperature profile is linear. The water mixing is absent since the water salinity is below the critical value 24.7 ppt.

a) b)

Figure 3. FBG and EBA thermistor strings in the ice tank (a) and in the ice bustle (b).

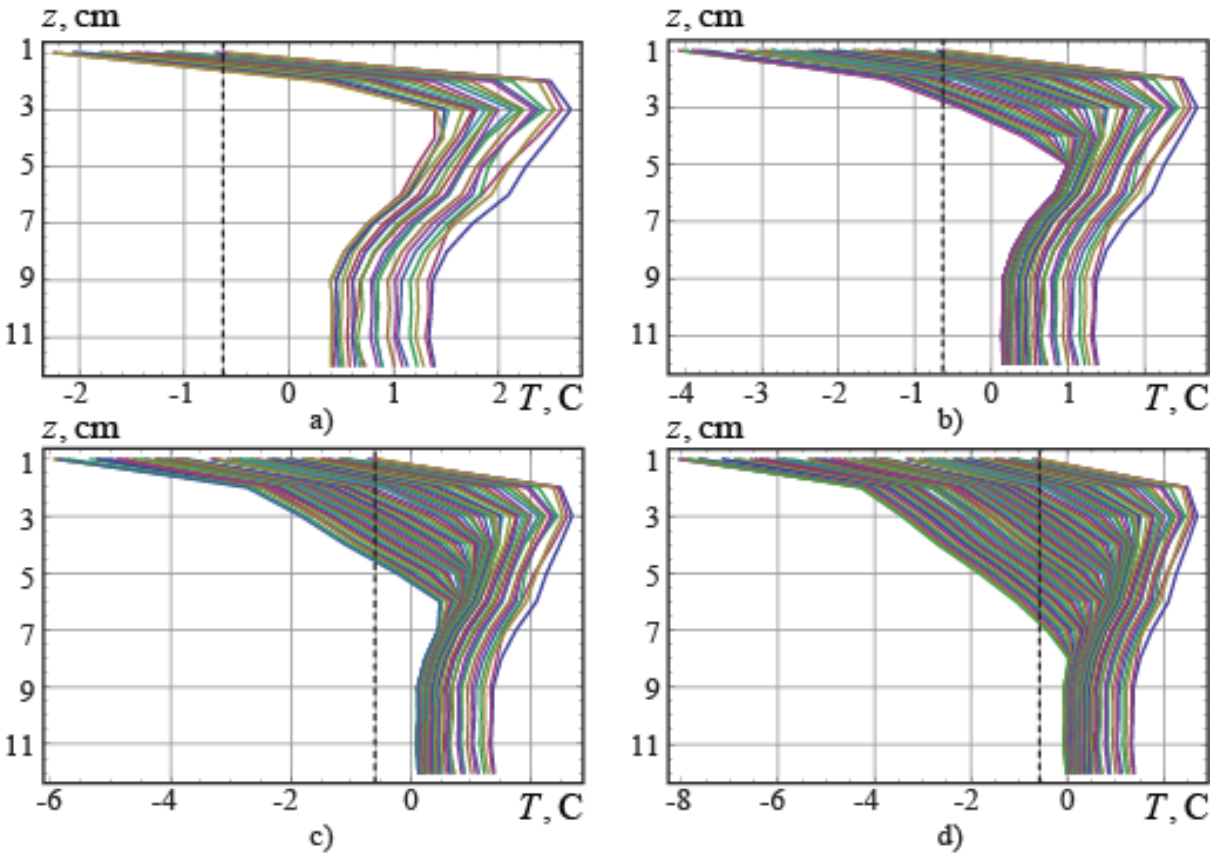

Figure 4. Temperature profiles measured during 6 h (a), 12 h (b), 18 h (c) and 24 h (d) after the beginning of the ice formation.

The experimental study of thermal changes in the ice under the influence of the water pressure variations was performed when the ice thickness was 9 cm. Temperature and pressure recorder SBE 39 placed on the tank bottom provided pressure measurements with initial accuracy 0.1% and resolution 0.002% of full scale range 20 m. Pressure record versus the time during the experiment is shown by blue line P in Fig. 5a. Temperature records from thermistors 3-8 are shown versus the time in the same figure by colour lines. Pressure and temperature records were performed both with 1 s sampling interval. Temperature profiles are shown in Fig. 5b for four times $t = 0$, 3, 5 and 13 min. Temperature variations with the amplitude about 0.1^{o}C corresponding to the pressure variations are visible in Fig. 5a. Temperature changes between $t = 5$ min and $t = 13$ min are very little, but the temperature increase detected by sensors 3-8 are still visible after $t = 8$ min. Air temperature changes recorded by sensor 1 at z= 1 cm visible in Fig. 5b were caused by the local influence of the door opening in the laboratory and changing of the ventilation.

The scheme of field experiment is shown in Fig. 2b. The thermistor string EBA with 16 equidistant sensors located on 20 cm distance from each other was mounted on supporting pile in the coal quay Kapp Amstedam in Svalbard on January 15, 2008. The thermistor string was placed inside steel pipe to avoid direct influence of the ice on the cable. The width of the ice bustle formed around the pile reached 1 m to the end of the March. Vertical extension of the ice bustles was about 1.5 m. The ice bustles are fixed on the piles and they are almost above the water surface in the low tide phase. When the water level is high the ice bustles are submerged in the water, and there is over pressure at the bottom of the ice bustle. Figure 3b shows the ice bustle and thermistor string in the February 2008.

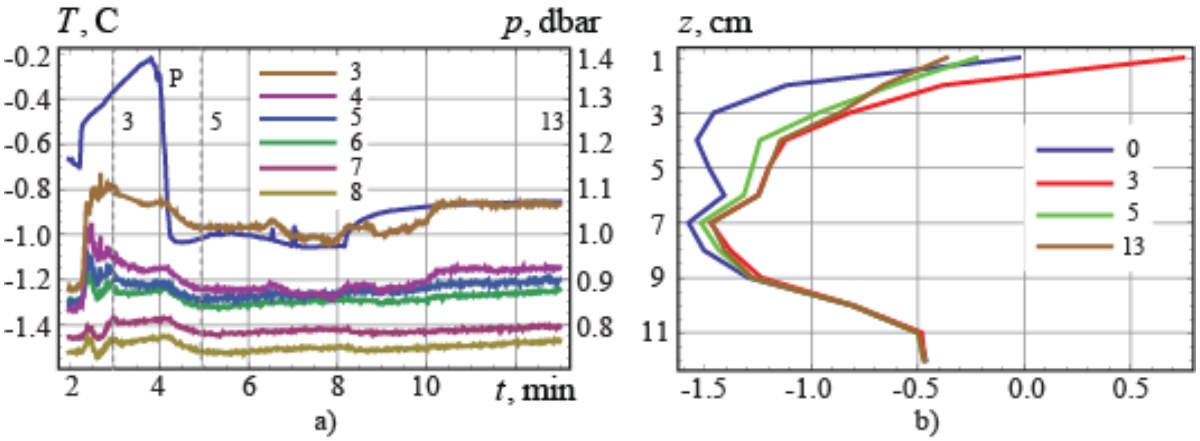

Figure 5. Records of the water pressure (P) and temperatures through the ice column versus the time (a). Temperature profiles through the ice column at times $t = 0,3,5$ and 13 min (b).

Figure 6a shows temporal variations of the water pressure at the sea bottom recorded with temperature and pressure recorder SBE 39 near the coal quay on February 14-15, 2008. Figures 6b-d show the variations of the temperature inside the ice recorded by thermistors 11 (b), 10 (c) and 9 (d) located in the lowest part of the ice bustle. Since the distance between thermistors is 20 cm, temperature variations induced by tide penetrate inside the ice bustle on the distance 60-70 cm.

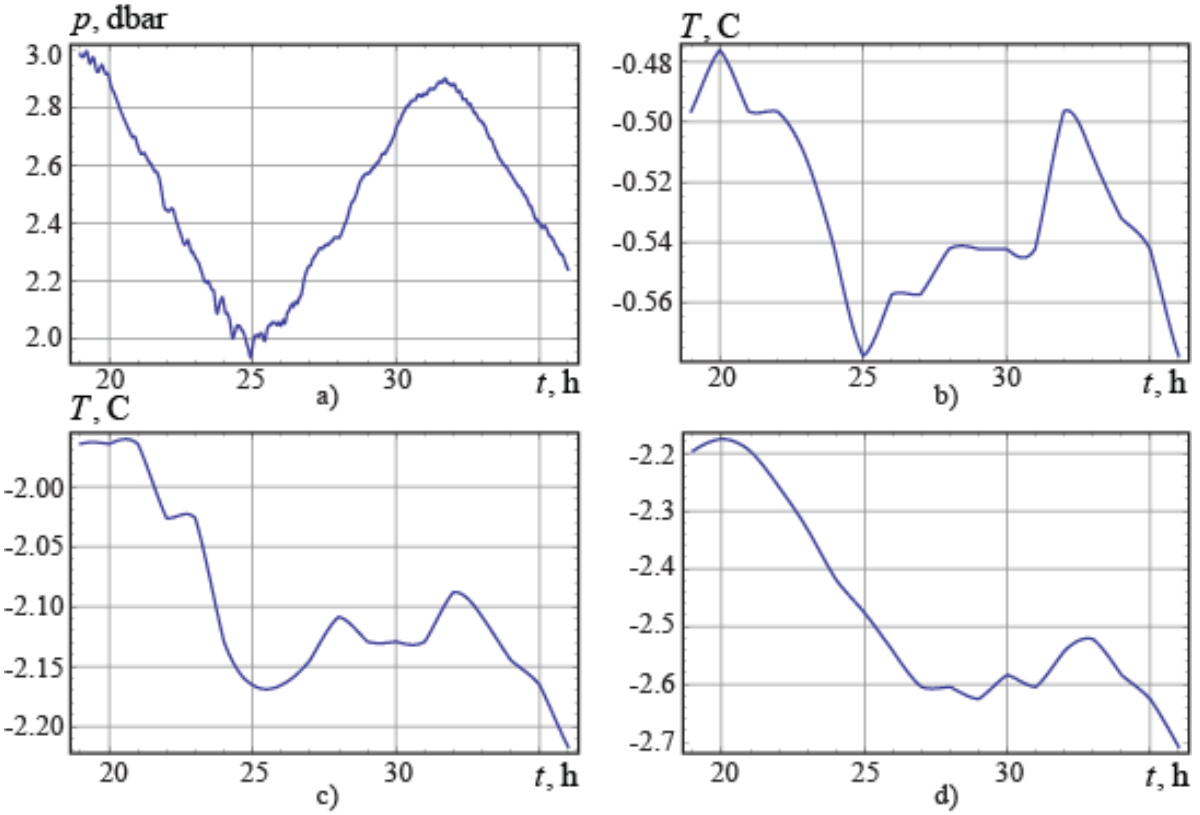

Figure 6. Tide induced variations of the water pressure at the bottom versus the time (a). Temperature variations measured in the lowest part of the ice bustle versus the time (b,c,d).

Thermal expansion of fresh and saline ice

Scheme of the laboratory experiment on thermal expansion of fresh and saline ice is shown in Fig. 7a. The extension of rectangular ice samples was measured with FBG strain sensor fixed

on the sides of the saw cut of the sample. Temperature profile was measured with FBG thermistor string placed in the middle of the sample in parallel direction to the fiber cable with the strain sensor. The sample was covered by plastic housing (Fig. 7b) to avoid an influence of the wind currents produced by fans. The length L of ice samples was 16-17 cm, the width and the altitude were about 10 cm.

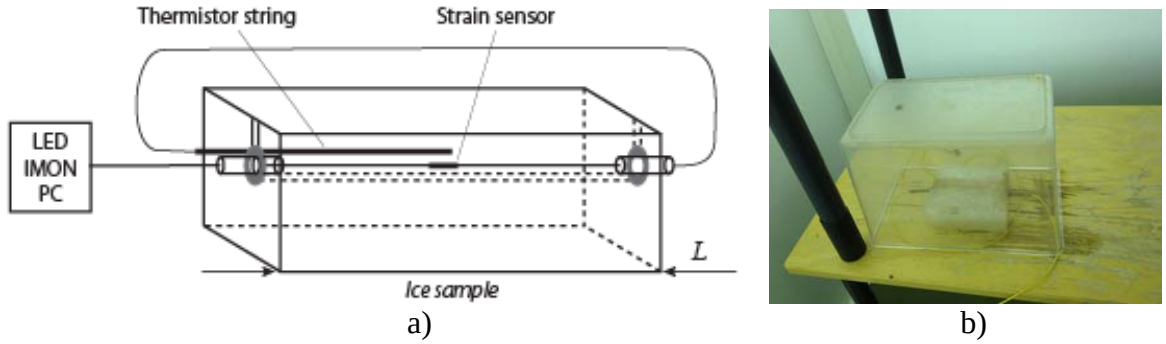

Figure 7. Scheme (a) and photograph (b) of experiment on thermal expansion of ice.

Temperature regulation in the cold laboratory is provided by coolers and fans beginning to work by a signal from temperature sensor mounted on the wall of the laboratory. Temperature changes in the laboratory are performed from the external selector box outside the laboratory. Three sets of different type experiments were performed. In the first set the temperature changed each two-three hours on two degrees. Duration of each of these tests was one-two days, and they are named as long-term tests. In the second set the temperature changed on 15^{o}-20^{o}C up and down in each test twice. Duration of such tests was 4-6 hours, and they are named as short-term tests. In the third set the cooling system switched off when the temperature in the laboratory was below -20^{o}C. In these tests the temperature in the laboratory increased more monotonically in comparison with the other tests.

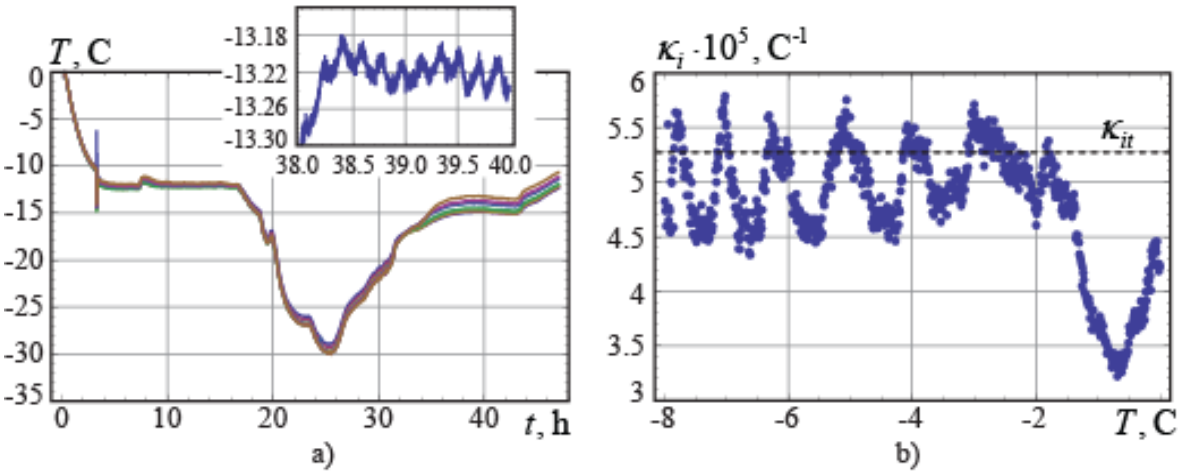

Figure 8. Temperature records versus the time (a) and the coefficient of thermal expansion versus the time (b) for fresh ice sample in long-term test.

Results of the long-term tests with fresh ice sample are shown in Fig. 8. Figure 8a demonstrates small temperature gradients over the ice sample in the long term tests. Small graph shows temporal variations of the temperature inside the sample induced by the fans work. Calculated values of the linear coefficient of thermal expansion (κ_i) shown in Fig. 8b by blue dots vary around the value $\kappa_{it} = 0.0000527$ C^{-1}, calculated with the formula

$$\kappa_{it} = -\frac{1}{3\rho_i}\frac{\partial \rho_i}{\partial T}, \qquad (1)$$

where fresh ice density is determined by the formula $\rho_i = 916.8(1+1.58\cdot 10^{-4}T)^{-1}$ (kg/m^3). The value κ_{it} is shown by dashed line in Fig. 8b.

Results of the long-term tests with saline ice sample are shown in Fig. 9a. The ice salinity calculated by the water salinity is about 6 ppt, but it can be greater because of the evaporation during the ice freezing. Blue and red dots show results of two different tests demonstrating the decrease of the linear coefficient of thermal expansion with the temperature increase. Blue line shows theoretical value (κ_{sit}) of the linear thermal expansion coefficient calculated with the formula

$$\kappa_{sit} = -\frac{1}{3\rho_{si}}\frac{\partial \rho_{si}}{\partial T}. \qquad (2)$$

Here sea ice density is calculated by the formula (Schwerdtfeger, 1963)

$$\rho_{si} = \frac{(1-\nu)\rho_w\rho_i\alpha T}{\sigma_{si}(\rho_i-\rho_w)+\rho_w\alpha T(1-\sigma_{si})}, \qquad (3)$$

where fresh water density is $\rho_w = 999$ kg/m^3, sea ice salinity is $\sigma_{si} = 0.006$, $\alpha = -0.0182$ C^{-1} and air bubble content is assumed equal to $\nu = 0$.

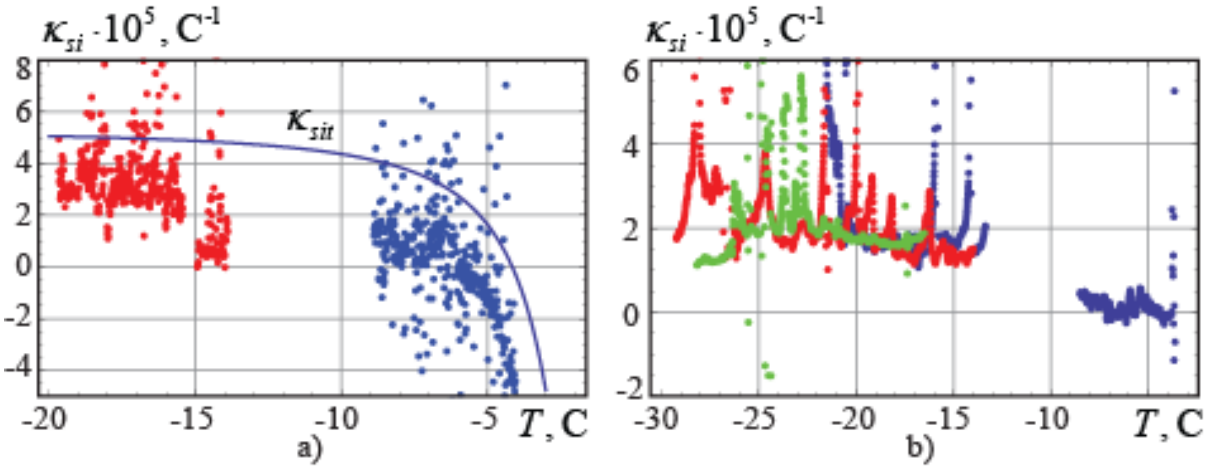

Figure 9. The coefficient of thermal expansion versus the time in long-term (a) and short-term (b) tests with saline ice. The ice salinity is 6 ppt.

Results of the short-term tests with the same sample of saline ice are shown in Fig. 9b. Mean values of the linear thermal expansion coefficients are lower in the short-term tests in comparison with the long-term tests, and the dispersion of the data is higher in the short-term tests. Results of the third type tests when the cooling system was switched off are shown in Fig. 10. The dispersion of the data is very little in comparison with previous tests. Experimental values of κ_{si} are very close to theoretical values κ_{sit} calculated with formula

(2) when the temperature is lower -4°C. The linear coefficient of thermal expansion decreases with the temperature increase and becomes negative around the temperature value $T \approx -4^{o}C$.

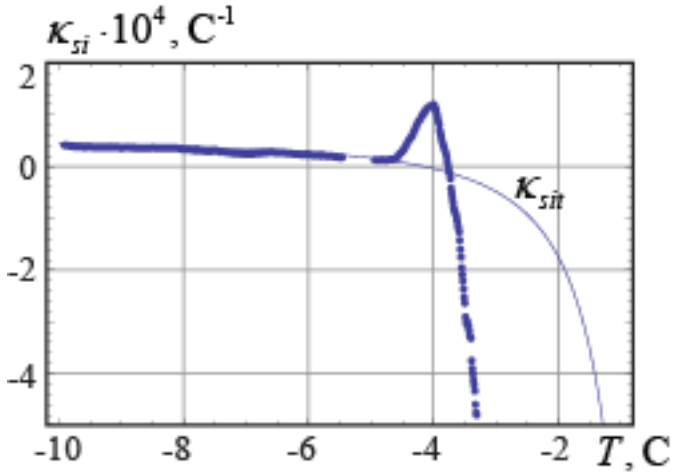

Figure 10. The coefficient of thermal expansion versus the time in the test when fans where switched off. The ice salinity is 6 ppt.

Conclusions

Performed experiments demonstrated advantages and disadvantages of FBG sensors for the measurement of physical processes in saline and fresh ice in laboratory conditions. Small sizes and high resolution of temperature and strain FBG sensors give possibility to freeze them in the ice with very small influence on the ice structure around the sensors at the scale of laboratory experiments. It also provides possibility to perform similar experiments in full and laboratory scales. Laboratory and full scale experiments showing temperature variations inside the ice induced by the water pressure variations below the ice demonstrate this approach. Observed temperature variations can be explained by vertical migration of liquid brine in porous space of saline ice. This effect could be stronger in the laboratory experiment if the process of the water pressure increase would be longer and more gradual. In the full scale the effect of tide induced temperature variations can be different in the ice frozen to the sheet piling and in the ice bustles. Results of these measurements will be collected and analysed later.

Experiments on thermal expansion have confirmed the decrease of the coefficient of thermal expansion of saline ice with the temperature increase. Experimental values of the thermal expansion coefficients are close to theoretical values determined by standard formula where the ice density accounts liquid brine in trapped porous space. In the temperature range below -5°C the coefficient of thermal expansion of fresh ice is higher than the coefficient of thermal expansion of saline ice with salinity 6 ppt. The coefficient of thermal expansion of saline ice is close to zero when the temperature is varying in the range from -5°C to -4°C.

Disadvantages of the use of the FBG sensors consist in the following. In some experiments numerous spikes in the thermistor string data were detected. They could be explained by different reasons: software problems, deformations of the thermistor string, influence of low temperatures and etc. For the current moment we don't have proven explanation and further analysis is required. Pretension of the FBG strain sensor in the ice sample required special technical experience and preparation of ice samples. Local ice deformations around places where the optical fiber is mounted on the ice sample can have an influence on the measurements.

References
Ferraro, P., De Natale, G., 2002. On the possible use of optical fiber Bragg gratings as strain sensors for geodynamical monitoring. Optics and Lasers in Engineering**, 37** (2-3), 115–130.
Johnson J.B., Metzner R.C., 1990. Thermal expansion coefficients for sea ice. Journal of Glaciology, 36(124), 343-349.
Løset, S., and A. Marchenko, 2009. Field Studies and Numerical Simulations of Ice Bustles on Vertical Piles. Cold Regions Science and Technology, 58, 15-28.
Malmgren, F., 1927. On the properties of sea ice. The Norwegian North Polar Expedition with the ”Maud”, 1918-1925, 1(5).
Marchenko, A., Thiel, T., Sukhorukov, S., 2012. Measurements of Thermally Induced Deformations in Saline Ice with Fiber Bragg Grating Sensors21st IAHR International Symposium on Ice "Ice Research for a Sustainable Environment", Li and Lu (ed.), Dalian University of Technology Press, Dalian, ISBN 978-7-89437-020-4, 651-659.
Marchenko, A., Shestov, A., Sigitov, A., Løset, S., 2011. Water-ice actions on the coal quay at Kapp Amsterdam in Svalbard. Proc. Int. Conf. Port Ocean Eng. Arct. Cond., POAC11-145, Montreal, Canada, 11 pp.
Mueller, B., Meissner, J., Thiel, T., 2006. Results of continuous in-situ stress measurement with optical strain sensors. In-situ Rock stress, London: Taylor & Francis Group, 249-256.
Othonos, A., Kalli, K., 1999. Fiber Bragg Gratings: Fundamentals and Applications in Telecommunications and Sensing. Artech House, ISBN 0-89006-344-3.
Rao, Y.J., 1997. In-fiber Bragg grating sensors. Measurement Science and Technology, 8(4), Sci. Technol., 8, 355-376.
Schwerdtfeger, P., 1963. The thermal properties of sea ice. Journal of Glaciology, Vol. 4, N 36, 789-807.
Sinitsyn, A., Wrangborg, D., Yulmetov, R., Sund, A.T., Marchenko, A., 2012. Measurements of Deformations and Displacements of Stationary Quays in Svalbard with 3D Laser Scanner Riegl VZ-1000. 21st IAHR International Symposium on Ice "Ice Research for a Sustainable Environment", Li and Lu (ed.), Dalian University of Technology Press, Dalian, ISBN 978-7-89437-020-4, 875-884.

Appendix
A Fiber Bragg Grating (FBG) is a periodical index change in the refractive index n along an optical silica fibre’s core, formed by an interference pattern of two UV laser beams that the fibre is exposed to (Fig. 11a). With a period of less than 10^{-6}mm, areas of higher n alternate with areas of lower n while Δn is relatively small ($\Delta n < 0.001$ *at* $n = 1.45$*)*. Due to the index change, each “grating line” reflects a very small portion of the light wave propagating along the fibre, back to the light source. Although a single reflected portion is negligible compared to the transmitted power, the effect becomes noticeable because the amount of “grating lines” in a conventional FBG is about 4000/mm, and a typical FBG with 10 mm length consists of 40 thousands reflections. If the light’s wavelength matches the condition

$$\lambda_{Bragg} = 2 \cdot n_{eff} \cdot \Lambda, \qquad \text{(A1)}$$

where n_{eff} is the fibre’s effective index, λ_{Bragg} is the light’s wavelength, and Λ is the index change’s period, then all reflected light wave portions are propagating “in-phase” and interfere constructively. Depending on the actual Δn, this results in a typical narrow-band power peak in the reflection spectrum at λ_{Bragg}, and vice versa in a loss in transmission (Fig. 11b). According to equation (1), the reflected wavelength changes with either modifying n_{eff} or Λ.

While Λ is meant as the distance between the grating lines, it is easy to see that λ_{Bragg} will change when the fiber is strained or compressed, whereas the effective refractive index is a material's property and thus n_{eff} is subject to changes in temperature. This sensitivity of the peak wavelength with respect to thermal and mechanical loads is utilized for the usage of FBG as strain and temperature sensors (Rao, 1997; Othonos, 1999) which nowadays encompasses a common field of optical sensing. Also in the field of Geophysics FBG sensing has been introduced with a remarkable attention due to several unique features that they provide (Ferraro 2002; Mueller, 2006). The main advantages of the FBG sensors embrace the long-term zero-point stability due to "inscribed" physical structure, a transmission of the sensor's signal over long distances up to tens of miles.

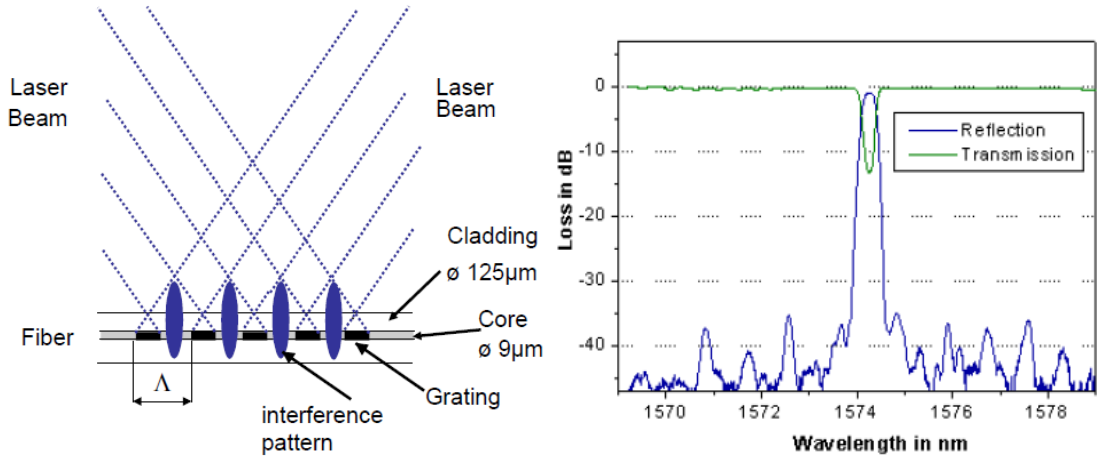

a) b)

Figure 11. Interference pattern of laser beams in the fiber core (a) during FBG generation. Broad band light travelling along the fibre with an FBG inside forming a typical pit in transmission and a peak in the reflection with the peak wavelength λ_{Bragg} (b). The light which is missing in the transmitted spectrum will be reflected to the light source.

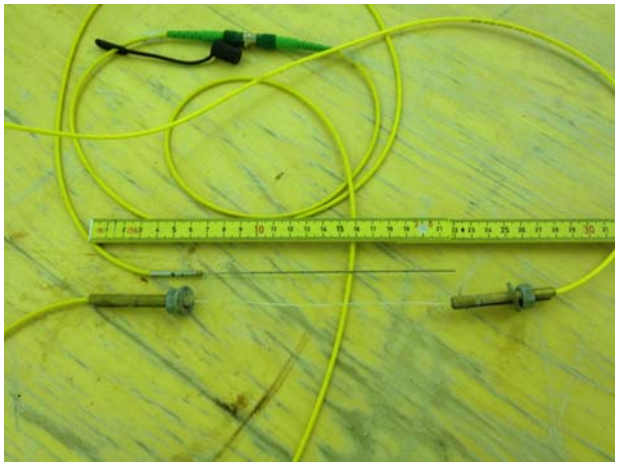

Figure 12. FBG thermistor string and strain sensor.

In our experiment, FBG sensors are very convenient for the measuring of thermal expansion of relatively large samples in contrast to standard dilatometers because the fiber can be embedded directly inside the ice sample. FBG thermistor string and starin sensor are shown in Fig. 12. The common strain resolution for FBG based sensing systems is better or equal 10^{-6} (1 µstrain), and the accuracy is typically $5 \cdot 10^{-6}$ (5 µstrain). These characteristics are

comparable with a Laser Dilatometers of Michelson Interferometer type used in the experiments of Johnson and Metzner (1990).

The variation ($\Delta\lambda_{Bragg}$) of the peak wavelength caused by the extension ($\Delta L / L$) and the change of the temperature (ΔT) of the sensor is described by the equation

$$\frac{\Delta\lambda}{\lambda} = GF \cdot \frac{\Delta L}{L} + TK \cdot \Delta T \,, \tag{A2}$$

where the gauge factor $GF = 0.719$ and a linear temperature coefficient $TK = 5.5 \cdot 10^{-6}$ are the constants obtained from a calibration cycle for our FBG sensors in standard SMF fiber, within a temperature range from -20^o C to 0^o C.

The variation of the peak wavelength $\Delta\lambda$ is measured with a spectrometer (Ibsen Photonics S/A, Denmark) that receives the reflected signal from the FBG sensor. For the calculation of the strain ($\Delta L / L$) according to formula (A2) it is necessary to measure the temperature change (ΔT) at the strain sensor's position in order to compensate *TK*. The temperature measurements can easily be performed with another FBG sensor protected from mechanical deforming, or alternatively with a thermometer. In our experiments, we used the FBG strain sensors with the reference peak wavelength in the vicinity of around 1534 nm, and the FBG temperature sensors with the reference peak wavelength in the range 1516-1588 nm. The strain and temperature sensors were cascaded in one optical fibre. The FBG measurement system's nominal resolution and accuracy in our experiment was 0.08^o C and 0.4^o C, respectively.